ORIGINAL ARTICLE

Basic Study

Green tea polyphenols alleviate di-(2-ethylhexyl) phthalate-induced liver injury in mice

Heng Shi, Xin-Hai Zhao, Qin Peng, Xian-Ling Zhou, Si-Si Liu, Chuan-Chuan Sun, Qiu-Yu Cao, Shi-Ping Zhu, Sheng-Yun Sun

Heng Shi, Xin-Hai Zhao, Xian-Ling Zhou, Chuan-Chuan Sun, Qiu-Yu Cao, Shi-Ping Zhu, Sheng-Yun Sun, Department of Traditional Chinese Medicine, The First Affiliated Hospital of Jinan University, Guangzhou 522000, Guangdong Province, China

Heng Shi, Qin Peng, Department of Gastroenterology, The Central Hospital of Shaoyang, Shaoyang 422000, Hunan Province, China

Si-Si Liu, Department of Pathology, The Central Hospital of Shaoyang, Shaoyang 422000, Hunan Province, China

Corresponding author: Sheng-Yun Sun, MD, PhD, Chief Doctor, Department of Traditional Chinese Medicine, The First Affiliated Hospital of Jinan University, No. 613 Huangpu Avenue West, Tianhe District, Guangzhou 522000, Guangdong Province, China. shengyunsun2020@163.com

Abstract

BACKGROUND

Di (2-ethylhexyl) phthalate (DEHP) is a common plasticizer known to cause liver injury. Green tea is reported to exert therapeutic effects on heavy metal exposure-induced organ damage. However, limited studies have examined the therapeutic effects of green tea polyphenols (GTPs) on DEHP-induced liver damage.

AIM

To evaluate the molecular mechanism underlying the therapeutic effects of GTPs on DEHP-induced liver damage.

METHODS

C57BL/6J mice were divided into the following five groups: Control, model [DEHP (1500 mg/kg bodyweight)], treatment [DEHP (1500 mg/kg bodyweight) + GTP (70 mg/kg bodyweight), oil, and GTP (70 mg/kg bodyweight)] groups. After 8 wk, the liver function, blood lipid profile, and liver histopathology were examined. Differentially expressed micro RNAs (miRNAs) and mRNAs in the liver tissues were examined using high-throughput sequencing. Additionally, functional enrichment analysis and immune infiltration prediction were performed. The miRNA-mRNA regulatory axis was elucidated using the starBase database. Protein expression was evaluated using immunohistochemistry.

RESULTS

GTPs alleviated DHEP-induced liver dysfunction, blood lipid dysregulation, fatty liver disease, liver fibrosis, and mitochondrial and endoplasmic reticulum lesions in mice. The infiltration of macrophages, mast cells, and natural killer cells varied between the model and treatment groups. mmu-miR-141-3p (a differentially expressed miRNA), *Zcchc24* (a differentially expressed mRNA), and Zcchc24 (a differentially expressed protein) constituted the miRNA-mRNA-protein regulatory axis involved in mediating the therapeutic effects of GTPs on DEHP-induced liver damage in mice.

CONCLUSION

This study demonstrated that GTPs mitigate DEHP-induced liver dysfunction, blood lipid dysregulation, fatty liver disease, and partial liver fibrosis, and regulate immune cell infiltration. Additionally, an important miRNA-mRNA-protein molecular regulatory axis involved in mediating the therapeutic effects of GTPs on DEHP-induced liver damage was elucidated.

Key Words: Green tea polyphenols; Di(2-ethylhexyl) phthalate; Liver fibrosis; Fatty liver disease; Mitochondria; Immune

Core Tip: Green tea polyphenols (GTPs) alleviated Di (2-ethylhexyl) phthalate (DEHP)-induced liver dysfunction, blood lipid dysregulation, fatty liver disease, liver fibrosis, and mitochondrial and endoplasmic reticulum lesions in mice. The infiltration of macrophages, mast cell, and natural killer cells varied between the model and treatment groups. mmu-miR-141-3p (a differentially expressed miRNA), *Zcchc24* (a differentially expressed mRNA), and Zcchc24 (a differentially expressed protein) constituted the miRNA-mRNA-protein regulatory axis involved in mediating the therapeutic effects of GTPs on DEHP-induced liver damage in mice.

INTRODUCTION

Di (2-ethylhexyl) phthalate (DEHP), which is the most widely used representative phthalic acid ester, can non-covalently bind to polyolefin plastics and predominantly serves as a plasticizer, increasing the flexibility, transparency, durability, and longevity of plastics. Additionally, DEHP is extensively detected in various daily-life products (including baby toys, food packaging, and cosmetics) and several surgical and medical devices[1]. Furthermore, DEHP can be continuously released into the environment (air, soil, water, food, *etc.*), enter living organisms *via* ingestion, inhalation, or skin contact, and subsequently exert toxic effects on health[2]. A previous study reported that DEHP and its metabolites were detected in 100% of tested human urine samples, indicating persistent exposure to DEHP[3]. The DEHP exposure range of the general population is estimated to be 5.8-19 μg/kg/d, while DEHP exposure in medical environments may exceed 167.9 mg/d[4]. The development of modern chemical agriculture has increased the severity of DEHP pollution. DEHP exposure in the Pearl River Delta region of Guangdong Province, China, can reach up to 61 μg/kg/d, which is higher than the tolerable intake of DEHP[5]. Additionally, DEHP undergoes rapid degradation upon ingestion in humans. According to the United States Environmental Protection Agency, the average half-life of DEHP in the human body is 12 h. DEHP and its active metabolite mono-(2-ethylhexyl) phthalate have been detected in various human tissues, including the liver, blood, placenta, amniotic fluid, and early-pregnancy chorionic villus sample[6]. Therefore, evaluating the effect of DEHP on the environment and human health has piqued the interest of the scientific community.

The liver, an important organ involved in the synthesis, metabolism, and detoxification processes, is highly susceptible to acute or chronic damage induced by various drugs[7]. Recent studies have demonstrated that DEHP adversely affects multiple systems in the body. In particular, epidemiological and animal studies have demonstrated the hepatotoxicity of DEHP[8]. The mechanism underlying the hepatotoxic effects of DEHP mainly involves oxidative stress, cell apoptosis, and signaling pathway activation. DEHP induces apoptosis in healthy human liver cells through the mitochondrial signaling pathway and/or the caspase-mediated death receptor pathway[9]. Additionally, DEHP may adversely affect gap junctional intercellular communication, peroxisome beta-oxidation activity, and DNA replication synthesis, leading to the formation of liver tumors[10]. Currently, the most extensively studied mechanism of DEHP-induced liver damage is oxidative stress in which the regulation of reactive oxygen species (ROS) production plays a critical role[11]. Excessive ROS production leads to peroxidation of the polyunsaturated fatty acids in the cell membrane. DEHP promotes lipid peroxidation in the liver, primarily through the downregulation of superoxide dismutase and catalase activity and the upregulation of malondialdehyde (MDA) concentrations[12]. Additionally, DEHP mediates the pathogenesis of non-alcoholic fatty liver disease in a high-fat diet-fed animal model by promoting lipid peroxidation[8].

Green tea is the second most widely consumed beverage worldwide after water[13]. The harvested tea leaves are steamed at high temperatures to inactivate the polyphenol oxidase in green tea, preserving most of the vitamins in tea leaves. Thus, green tea exhibits enhanced antioxidant activity. Epidemiological and clinical studies have reported that phenol compounds in tea extracts, such as green tea polyphenols (GTPs), exert a wide range of beneficial effects on human health, including anti-aging, neuroprotective[14], and therapeutic or preventive effects on various diseases, such as cancer[15], cardiovascular disease[16], and obesity[17]. Moreover, GTPs mitigate the adverse effects of poisoning with various heavy metals[18]. However, limited studies have examined the therapeutic effects of GTPs on DEHP-induced liver diseases.

Micro RNAs (miRNAs), a class of endogenous non-coding small RNAs encoded by mRNA, regulate gene expression by modulating mRNA stability. Several miRNAs are reported to play important roles in the pathogenesis of liver fibrosis [19], cirrhosis[20], and hepatocellular carcinoma[21]. Some miRNAs are diagnostic markers for drug-induced liver injury [22]. This study aimed to identify key protein nodes that may affect the expression level of miRNAs in the regulatory network of miRNA and target genes by analyzing the miRNA regulation network. Hence, this study will provide a theoretical basis for future studies on the functions and regulatory mechanisms underlying the therapeutic effects of GTPs on DEHP exposure-induced liver damage.

MATERIALS AND METHODS

Regents
DEHP was purchased from Shanghai Aladdin Biochemical Technology Co., Ltd. (Shanghai, China). GTPs were purchased from Shanghai Yuanye Bio-Technology Co., Ltd. (Shanghai, China). Corn oil was purchased from Hebei Pin Research Biotechnology Co., Ltd. (Baoding, China). Anti-ZCCHC24 antibodies were purchased from Biorbyt Ltd. (Cambridge, United Kingdom).

Animal experiments
Animal experiments were performed at the specific pathogen-free grade animal laboratory of the Medical College of Jinan University. C57BL/6J mice (n = 50) were purchased from Guangdong Yaokang Biotechnology Co., Ltd. And allowed to acclimatize to the laboratory environment for 1 wk. The animals were maintained under the following conditions: Room temperature, 20 °C-24 °C; relative humidity, 50%-65%; circadian cycle, 12-h light-dark cycle; access to food and water, ad libitum; diet, regular mouse chow. This study was approved by the Institutional Animal Care and Use Committee of Jinan University (ethics approval number: IACUC-20210630-15). All experimental procedures were performed according to the regulations established by the ethical committee.

Previous studies[23,24] have reported that DEHP is soluble in corn oil. Hence, this study used corn oil as the solvent for DEHP. After 1 wk of acclimatization, 50 mice were randomly assigned into the following five groups (10 mice/ group): Control group, administered with 0.2 mL distilled water; model group, administered with 0.2 mL corn oil and DEHP (1500 mg/kg bodyweight); treatment group, administered with 0.2 mL corn oil and DEHP (1500 mg/kg bodyweight), followed by administration of 0.2 mL GTPs (70 mg/kg bodyweight) after 1 h; oil group, administered with 0.2 mL corn oil; GTP group, administered with 0.2 mL GTP (70 mg/kg bodyweight). Based on our previous study, DEHP [25] and GTPs[26] were gavaged. The doses were adjusted weekly based on the bodyweight of the mice. The mice were subjected to daily gavage for 8 wk. At the end of the experimental period, the blood and liver samples were obtained under anesthesia after the mice were allowed to fast overnight. Liver index = (liver weight/bodyweight) × 100%.

Evaluation of liver function and blood lipid profile
The blood from mice was collected using the retro-orbital venous plexus method. Next, the whole blood was placed in a 1.5-mL centrifuge tube and left undisturbed at room temperature for 2 h. The sample was centrifuged at 5 °C and 3000 rpm for 15 min using a high-speed refrigerated centrifuge to obtain the serum. The serum levels of liver function markers [aspartate aminotransferase (AST), alanine aminotransferase (ALT), and total bilirubin (TBIL)] and lipids [low-density lipoprotein (LDL), total cholesterol, and triglycerides (TGs)] were analyzed using a fully automated biochemical analyzer.

Hematoxylin and eosin staining
The tissue sections were fixed in 4% neutral buffered formalin, embedded in paraffin, and sectioned into 4 μm-thick sections. The sections were deparaffinized using xylene, rehydrated using a series of graded ethanol solutions, stained with hematoxylin for 5–10 min, washed with distilled water, and stained with eosin for 2-7 min. Next, the sections were dehydrated using a series of graded ethanol solutions, cleared with xylene, mounted with mounting medium, and covered with a cover slip.

Oil red O staining
The frozen sections were fixed in 4% neutral buffered formalin, rinsed with 60% isopropanol, and allowed to dry. The sections were then stained with oil red O for 15-30 min, rinsed with 60% isopropanol, counterstained with hematoxylin for 1-2 min, washed with distilled water, dehydrated, mounted with a mounting medium, and covered with a coverslip.

Periodic acid-Schiff staining
The tissue sections were deparaffinized using xylene, rehydrated using a series of graded ethanol solutions, and oxidized

with a periodic acid solution for 10-15 min. Next, the sections were rinsed with distilled water, stained with Schiff reagent for 30-60 min in the dark, counterstained with hematoxylin, washed with distilled water, dehydrated, mounted using a mounting medium, and covered with a cover slip.

Masson's trichrome staining

The tissue sections were deparaffinized using xylene, rehydrated using a series of graded ethanol solutions, stained with Weigert's iron hematoxylin for 10 min, rinsed with distilled water, stained with Biebrich scarlet-acid fuchsin solution for 5-10 min, washed with distilled water, and incubated with phosphotungstic-phosphomolybdic acid solution for 5-10 min. Next, the sections were counterstained with aniline blue for 5-10 min, washed with distilled water, dehydrated, mounted with a mounting medium, and covered with a cover slip.

Sirius red staining

The tissue sections were deparaffinized using xylene, rehydrated using a series of graded ethanol solutions, stained with Sirius red solution for 1 h, washed with distilled water, dehydrated, and cleared with xylene. Finally, the sections were mounted with a mounting medium and covered with a cover slip.

Transmission electron microscopy

One mouse from the control, treatment, and model groups was randomly selected for electron microscopy. Liver sections with a size of approximately 1 mm were treated with 2.5% glutaraldehyde (Scientific Phygene, Fuzhou, China) and rinsed thrice with phosphate-buffered saline (PBS) (PH = 7.4). The samples were fixed with 1% osmium tetroxide (Ted Pella, Redding, United States) for 2 h, rinsed thrice with PBS, and dehydrated using alcohol and acetone gradients as follows: 50% ethanol for 30 min, 70% ethanol for 30 h, 80% acetone for 30 min, and 90% acetone for 30 h. Next, the samples were washed thrice with 100% acetone and embedded in epoxy resin (Ted Pella, Redding, United States). Ultrathin sections (7 nm) were prepared using a microtome (LKB, Bromma, Sweden). The sections were stained with uranyl acetate (EMS, Hatfield, United States) for 30 min and 3% lead citrate (Ted Pella, Redding, United States) for 15 min. The target structures were observed using a transmission electron microscope (JEM-1400, Japan Electron Optics Laboratory Co., Ltd. Tokyo, Japan).

High-throughput sequencing

Liver samples (n = 3 per group) from the control, treatment, and model groups stored in liquid nitrogen were randomly selected and sent to Huada Genomics (Wuhan, China, http://www.genomics.cn) for high-throughput sequencing. For specific sequencing steps, refer to the Supplementary material.

Differentially expressed mRNAs and miRNAs

The mRNA and miRNA expression levels were measured using fragments per kilobase of transcript per million mapped reads (FPKM) values. Sequencing data were subjected to quality control. Differential expression between groups was estimated using the Limma R package (version: 3.52.2) based on the generalized linear model. To comparatively analyze the expression levels between multiple groups, the control-model and model-treatment expression profiles were regressed using the Limma package in R software (version: 4.2.1, https://posit.co/). A loose threshold was set to avoid excessive filtering of differentially expressed mRNAs and miRNAs (log fold-change > 1; $P < 0.05$). Differentially expressed mRNAs and miRNAs were identified.

Enrichment analysis

The mRNA expression data were subjected to Gene Ontology (GO) and Kyoto Encyclopedia of Genes and Genomes (KEGG) pathway analyses to identify the enrichment of mRNAs in the GO terms biological process (BP), cellular component (CC), and molecular function (MF) and the KEGG signaling pathways. The clusterprofiler R package (version: 4.4.4) was used for enrichment analyses with the reference files based on the org.Mm.eg.db R package (version 3.1.0) for mouse enrichment analysis. Enrichment was considered significant at $P < 0.05$.

Immune infiltration analysis

CIBERSORT is a gene expression-based algorithm for the accurate detection of immune cell infiltration. The "CIBERSORT" R package (CIBERSORTR script v1.03; http://cibersort.stanford.edu/) developed by Newman *et al*[27] was used to successfully quantify 22 types of immune cells, including B cells, regulatory T cells, CD4+ T, CD8+ T, natural killer (NK) cells, mast cells, plasma cells, dendritic cells, neutrophils, eosinophils, and macrophages. The reference dataset of mouse immune cells was obtained from Chen *et al*[28]. The mRNA expression data of the control, model, and treatment groups were examined using the CIBERSORT algorithm with a perm of the deconvolution algorithm set to 1000.

Regulatory network of miRNA-mRNA

miRNA, a type of non-coding RNA, negatively regulates gene expression at the posttranscriptional level. To generate a preliminary regulatory network of miRNA-mRNA in the model and treatment groups, the upregulated miRNAs or mRNAs and downregulated mRNAs or miRNAs were selected and analyzed using Cytoscape software (version: 3.7.1, https://cytoscape.org/).

The Sun Yat-sen University research team developed the starBase database (https://starbase.sysu.edu.cn/starbase2/) to analyze interaction networks between long non-coding RNA, miRNA, competitive endogenous RNAs, RNA-binding proteins, and mRNAs using cross-linked immunoprecipitation sequencing (CLIP-seq) (high-throughput sequencing of RNA using CLIP, photoactivable ribonucleoside-enhanced CLIP, individual nucleotide resolution ultraviolet CLIP, and cross-linking ligation and sequencing of hybrids) data. To obtain the final miRNA-mRNA regulatory network, the initially selected network was intersected with the mouse interaction network obtained from the starBase database. Gene expression was verified using immunohistochemical analyses. This study aimed to establish the miRNA-mRNA-protein regulatory axis.

Immunohistochemistry
The paraffin sections (4 μm) of mouse liver tissue were deparaffinized, rehydrated, and subjected to antigen retrieval in a buffer solution (pH 9.0). After blocking endogenous peroxidase activity and non-specific binding, the sections were incubated with anti-ZCCHC24 antibodies (1:100) at 4 °C overnight. The sections were then washed and incubated with horseradish peroxidase-conjugated secondary antibodies at room temperature for 1 h. Immunoreactive signals were developed using diaminobenzidine. The sections were counterstained with hematoxylin and observed under a microscope.

Statistical analyses
The average optical density (AOD) (integrated optical density/area) of positive reactions was calculated using Image-Pro Plus 6.0 software. Data were analyzed using the dplyr R package (v. 1.0.10) and visualized using the ggplot2 R package (v. 3.3.6). Categorical variables were analyzed using the Chi-squared test. Continuous variables were represented as mean ± SD. Continuous variables between two groups were compared using the Wilcoxon signed-rank test, while those between more than two groups were compared using the Kruskal-Wallis test. Differences were considered significant at $P < 0.05$.

RESULTS

Effect of GTPs on bodyweight and liver index
The flowchart of the study is shown in Figure 1. Mice in all groups survived during the experiment and did not exhibit aberrant behaviors in urination, defecation, food intake, or water consumption. As shown in Supplementary Table 1 and Figure 2A, the bodyweight of mice in all groups increased with time and was not significantly different between the groups. The liver index (Supplementary Table 2 and Figure 2B) values in the model group were significantly higher than those in the control group ($P = 0.016$) but were not significantly different between the treatment and model groups ($P = 0.51$). Additionally, the liver index values in the oil and GTP groups were not significantly different from those in the control group ($P > 0.05$).

Effect of GTPs on the serum levels of liver function markers and lipids
The serum levels of ALT, AST, TBIL, LDL, and TGs were analyzed. As shown in Figure 2C-G, the serum levels of ALT, AST, TBIL, LDL, and TGs in the model group were significantly higher than those in the control group ($P < 0.001$). Compared with those in the model group, the serum levels of liver function markers and lipids were significantly downregulated in the treatment group ($P < 0.001$). The ALT, AST, and LDL levels were not significantly different between the oil, control, and GTP groups ($P > 0.05$).

Effect of GTPs on hepatic histological characteristics
The results of liver hematoxylin and eosin staining are shown in Figure 3A. Mice in the model group exhibited significant hepatocyte ballooning degeneration, whereas those in the control, oil, and GTP groups did not exhibit hepatocyte ballooning degeneration.

Effect of GTPs on fat deposition
Oil red O staining was performed to further analyze the severity of fatty liver in different groups. As shown in Figure 3A, the model group exhibited the highest red color staining intensity in the liver, followed by the oil and control groups. Meanwhile, the liver of the treatment and GTP groups exhibited the lowest red staining intensity. Five positive staining sites in the liver of the model and treatment groups were selected to calculate the AOD. As shown in Figure 3B, the AOD in the model group (7.270 ± 1.120%) was significantly higher than that in the treatment (0.185 ± 0.061%) ($P = 0.037$) and control groups (5.760 ± 0.586%) ($P < 0.001$).

Effect of GTPs on polysaccharide accumulation
The results of Periodic acid-Schiff staining (Figure 3A) revealed the lack of red-stained areas in the liver of the model group, while the red-stained areas were upregulated in the control, oil, treatment, and GTP groups. Five positive staining sites in the liver of the model and treatment groups were selected to calculate the AOD. As shown in Figure 3C, the AOD in the model group (0.431 ± 0.083%) was significantly lower than that in the treatment (1.170 ± 0.099%) and control groups (1.360 ± 0.148%) ($P < 0.001$).
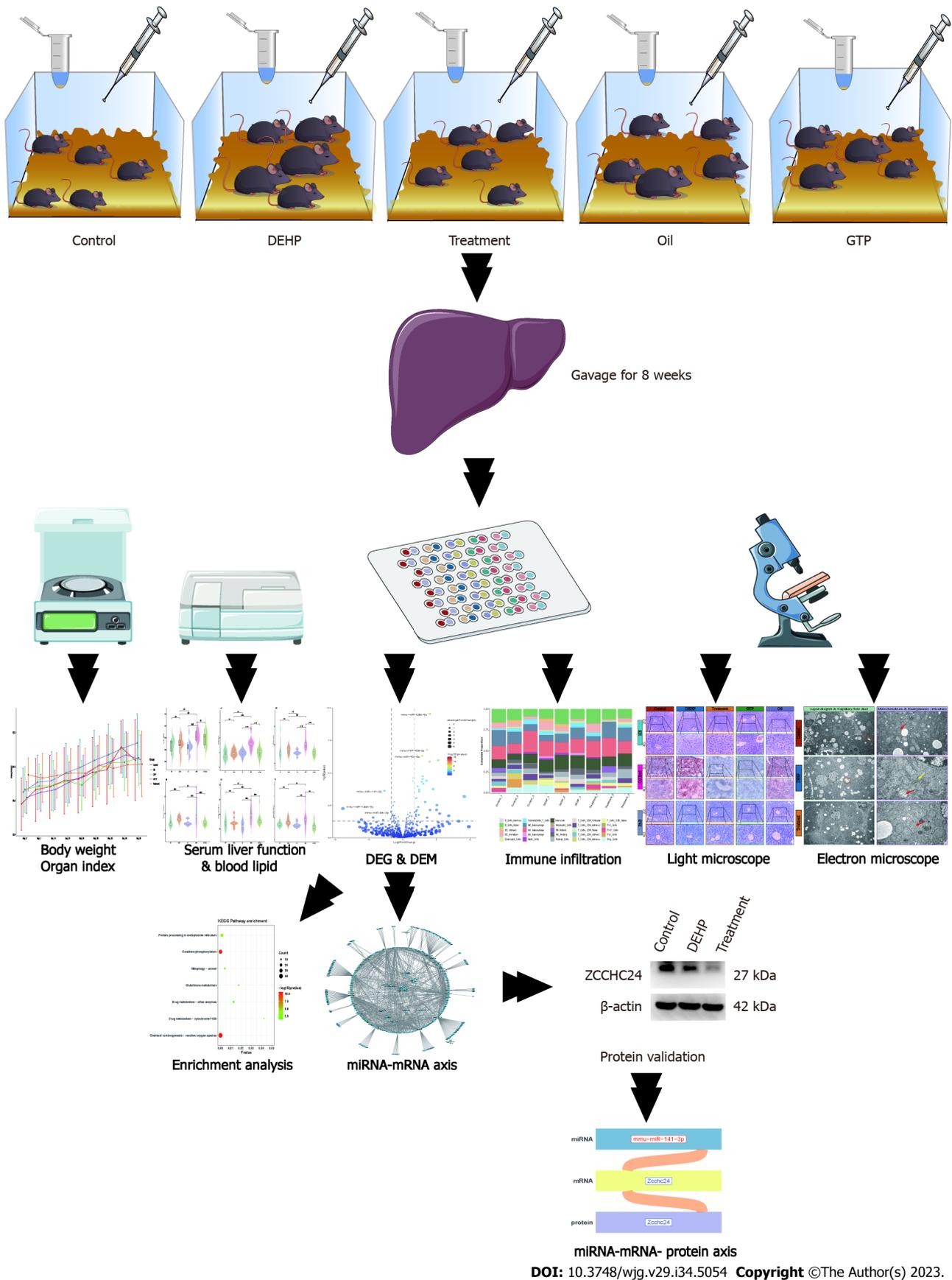
Figure 1 Flowchart of the study. DEG: Differentially expressed gene; DEM: Differentially expressed microRNA (miRNA).

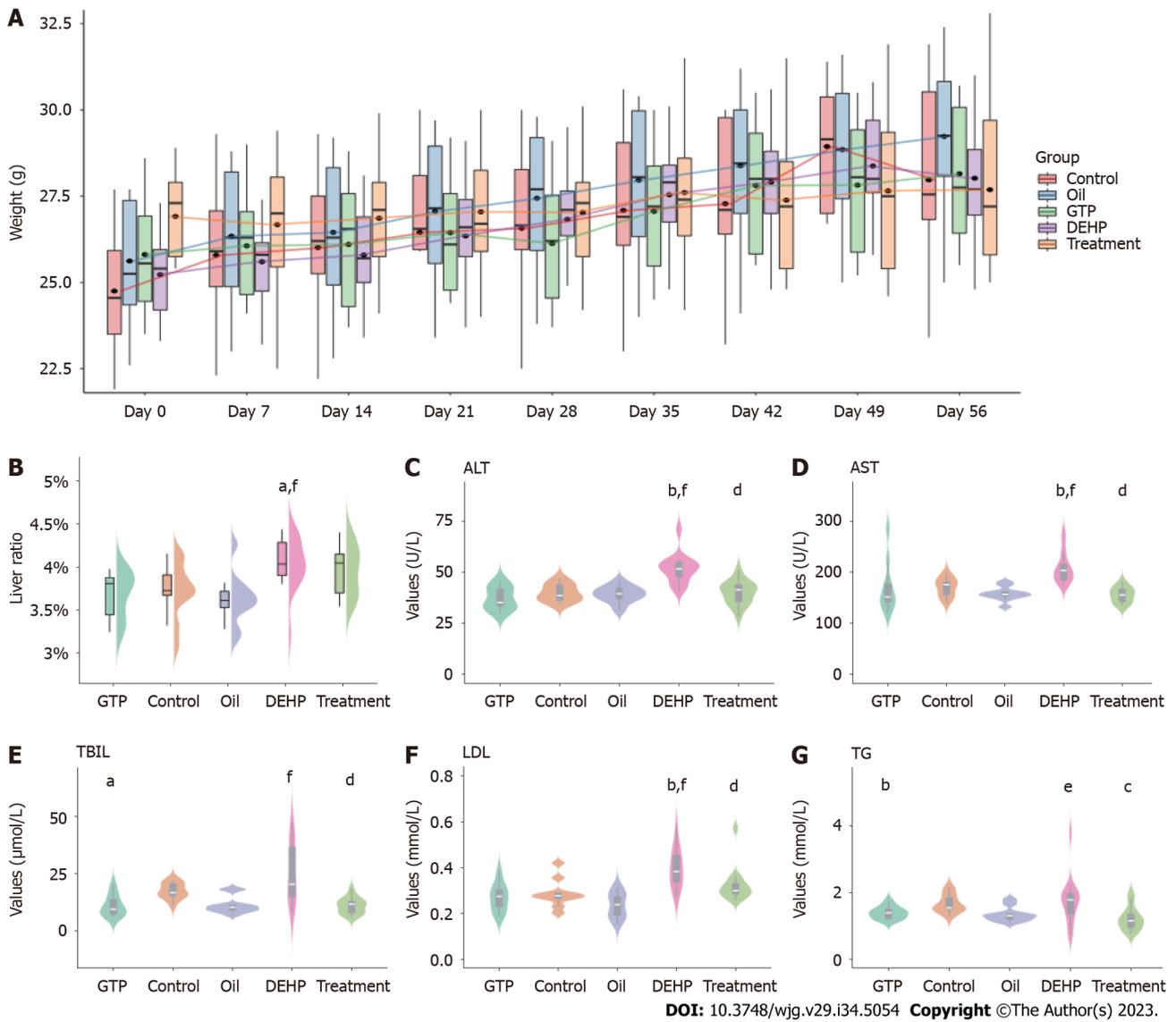**DOI:** 10.3748/wjg.v29.i34.5054 **Copyright** ©The Author(s) 2023.

Figure 2 Mouse bodyweight and liver index and serum levels of liver function markers and lipids. A: Bodyweight changes in different groups within 8 wk; B-G: Comparative analysis of organ indices (B) and serum levels of alanine aminotransferase (C), glutamate aminotransferase (D), total bilirubin (E), low-density lipoprotein (F), and triglyceride (G) in different groups. [a]$P < 0.05$ and [b]$P < 0.01$ (compared to the Control group); [c]$P < 0.05$ and [d]$P < 0.01$ (compared to Di (2-ethylhexyl) phthalate group); [e]$P < 0.05$ and [f]$P < 0.01$ (compared to Oil group). ALT: Alanine aminotransferase; AST: Glutamate aminotransferase; TBIL: Total bilirubin; LDL: Low-density lipoprotein; TG: Triglyceride; DEHP: Di (2-ethylhexyl) phthalate.

Effect of GTPs on collagen fibers

The results of Masson's trichrome staining (Figure 4A) revealed blue-stained fibrous tissue around the liver blood vessels in the model group. In contrast, the area of blue-stained fibrous tissue around the liver blood vessels in the treatment group was lower than that in the model group. Fibrous tissue was not detected around the liver blood vessels in the control, oil, and GTP groups. Five positive staining sites in the liver of the model and treatment groups were selected to calculate the AOD. As shown in Figure 4B, the AOD in the model group ($0.337 \pm 0.113\%$) was significantly higher than that in the treatment group ($0.183 \pm 0.014\%$) ($P = 0.02$).

Effect of GTPs on collagen network

In Sirius red staining, type I collagen fibers exhibit strong orange-yellow or bright red colors under a polarized light microscope, whereas type III collagen fibers exhibit green color. In this study, the results of Sirius red staining (Figure 4A) revealed red-stained fibrous tissue around the blood vessels in the model group. The red-stained area around the blood vessels in the treatment group was significantly lower than that in the model group. Red-stained fibrous tissue was not detected around the blood vessels of the control, oil, and GTP groups. Next, semiquantitative analysis was performed by selecting five positive staining sites in the liver of the model and treatment groups to calculate the AOD. The AOD in the model group ($1.240 \pm 0.125\%$) was significantly higher than that in the treatment group ($0.080 \pm 0.025\%$) ($P = 0.012$) (Figure 4C).
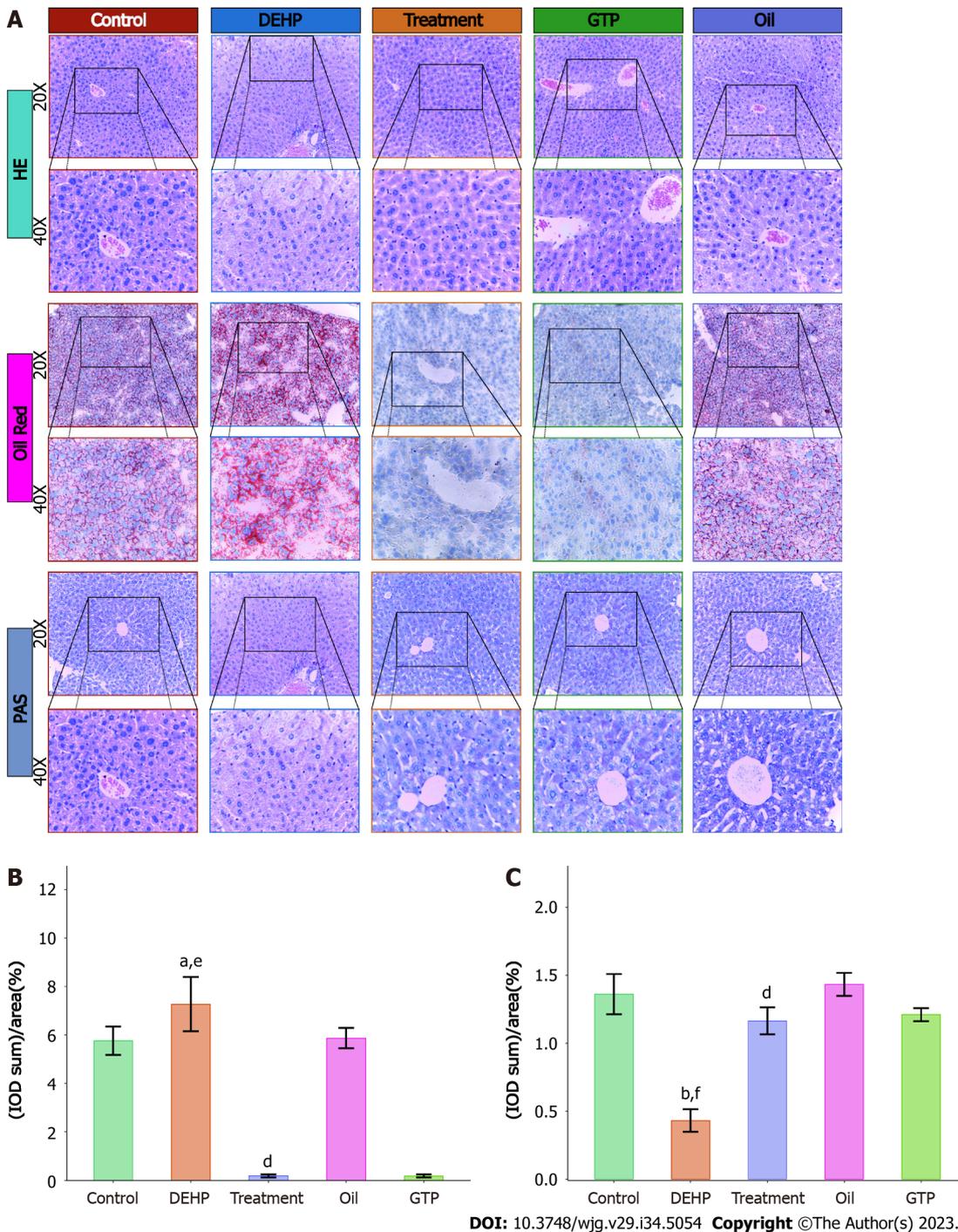
Figure 3 Hematoxylin and eosin, oil red O, and periodic acid-Schaff staining of liver sections and semiquantitative analysis of liver pathologies in mice from different groups. A: Hematoxylin and eosin-stained, oil red O-stained, and periodic acid-Schaff (PAS)-stained liver sections of different groups; B and C: Comparative analysis of average optical density of oil red O staining (B) and PAS staining (C) intensities between different groups. $^{a}P <$ 0.05 and $^{b}P <$ 0.01 (compared to the Control group); $^{d}P <$ 0.01 (compared to Di (2-ethylhexyl) phthalate group); $^{e}P <$ 0.05 and $^{f}P <$ 0.01 (compared to Oil group). DEHP: Di (2-ethylhexyl) phthalate; HE: Hematoxylin and eosin; PAS: Periodic acid-Schaff.

DOI: 10.3748/wjg.v29.i34.5054 **Copyright** ©The Author(s) 2023.

Effect of GTPs on the liver microstructures

The liver tissues of the control, model, and treatment groups were subjected to transmission electron microscopy. The number and size of lipid droplets in the liver were upregulated and the capillary bile ducts were significantly dilated in the model group (Figure 5A). Additionally, the mitochondria were slightly swollen, and the arrangement of the rough endoplasmic reticulum was disordered. In contrast, the number of lipid droplets in the liver was downregulated in the treatment group, while the capillary bile ducts exhibited physiological structure. Additionally, the swelling of the mitochondria was alleviated. The results of quantitative analysis of the diameter of small bile ducts (Figure 5B) were consistent with the observations in Figure 5A. However, these findings must be carefully interpreted. Additionally, further studies with large sample sizes are needed to confirm and generalize the results.
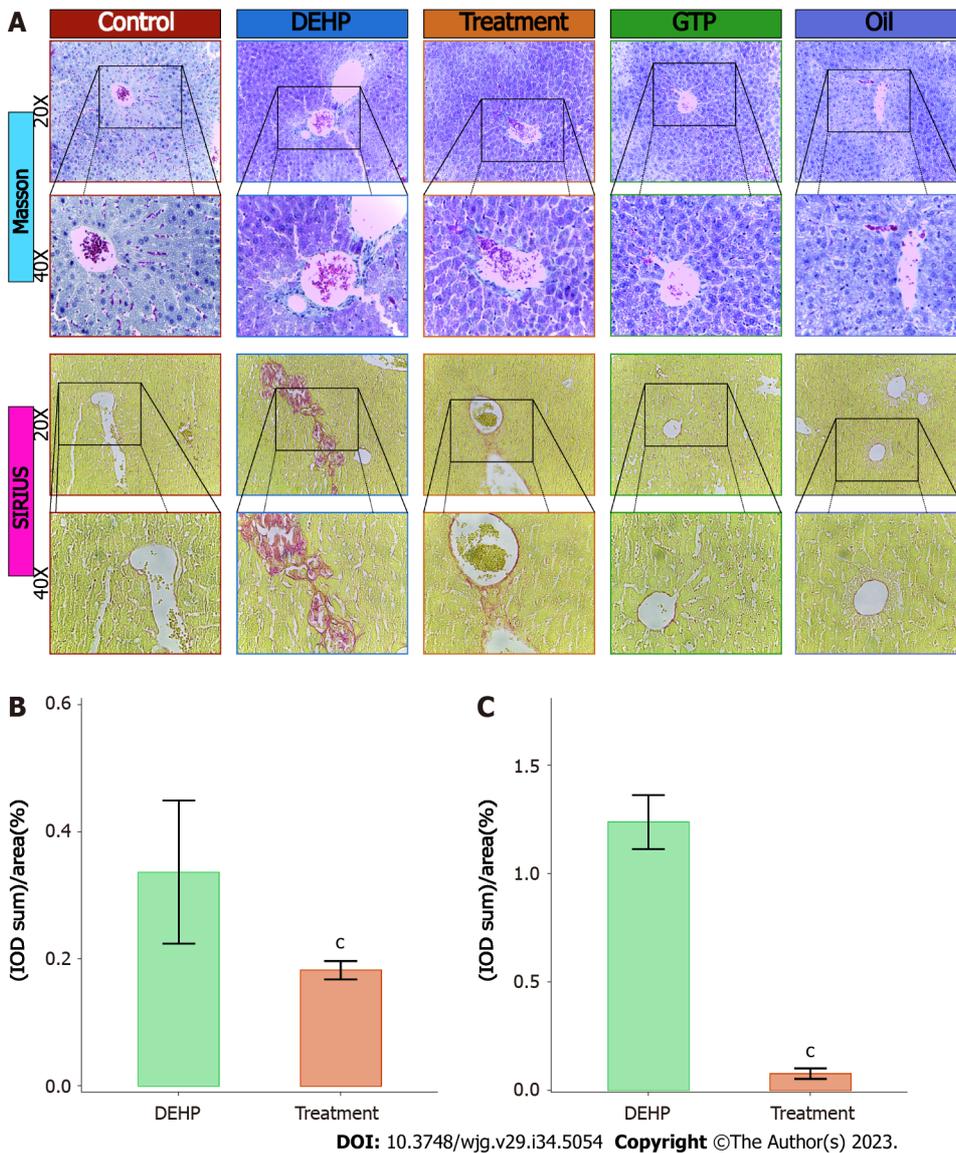
Figure 4 Masson's trichrome and Sirius red staining and semiquantitative analysis of hepatic pathologies in mice from different groups.
A: Masson's trichrome and Sirius red staining of liver samples from different groups; B and C: Comparative analysis of average optical density of Masson's trichrome staining (B) and Sirius red staining (C) intensities between the model and treatment groups. $^{c}P < 0.05$ (compared to Di (2-ethylhexyl) phthalate group). DEHP: Di (2-ethylhexyl) phthalate.

Effect of GTPs on mRNA and miRNA expression levels

The liver samples from the control, treatment, and model groups were subjected to high-throughput screening with 3 replicate samples for each group. The mRNA and miRNA expression data were subjected to quality control analysis. The differences in the expression levels of miRNA and mRNA were minimal between the groups (Supplementary Figure 1A and B). Next, principal component analysis was performed (Supplementary Figure 1C and D). The mRNA and miRNA profiles of the control, model, and treatment groups exhibited distinct separation. Differential analysis revealed that compared with those in the model group, the number of upregulated mRNAs and miRNAs was 377 and 33, respectively, while the number of downregulated mRNAs and miRNAs was 583 and 7, respectively (Figure 6A and B). The expression levels of the significantly upregulated and downregulated mRNAs and miRNAs are shown in Figure 6C and D.

Enrichment analyses

Compared with those in the control group, the differentially expressed mRNAs in the model group were enriched in the following GO terms: BP term: Fatty acid metabolic process, small molecule catabolic process, organic acid catabolic process, and carboxylic acid catabolic process (Figure 7A); CC term: Mitochondrial protein-containing complex, mitochondrial inner membrane, ribosome subunit, and ribosome (Figure 7B); MF term: Ribosome structure, electron transfer activity, oxidoreductase activity, and ubiquitin protein ligase binding (Figure 7C). Additionally, the differentially expressed mRNAs in the model group were enriched in the following KEGG pathways: Fatty acid metabolism, ferroptosis, glutathione metabolism, and PPAR signaling pathway (Figure 7D). Compared with those in the model group, the differentially expressed mRNAs in the treatment group were enriched in the following GO terms: BP term:
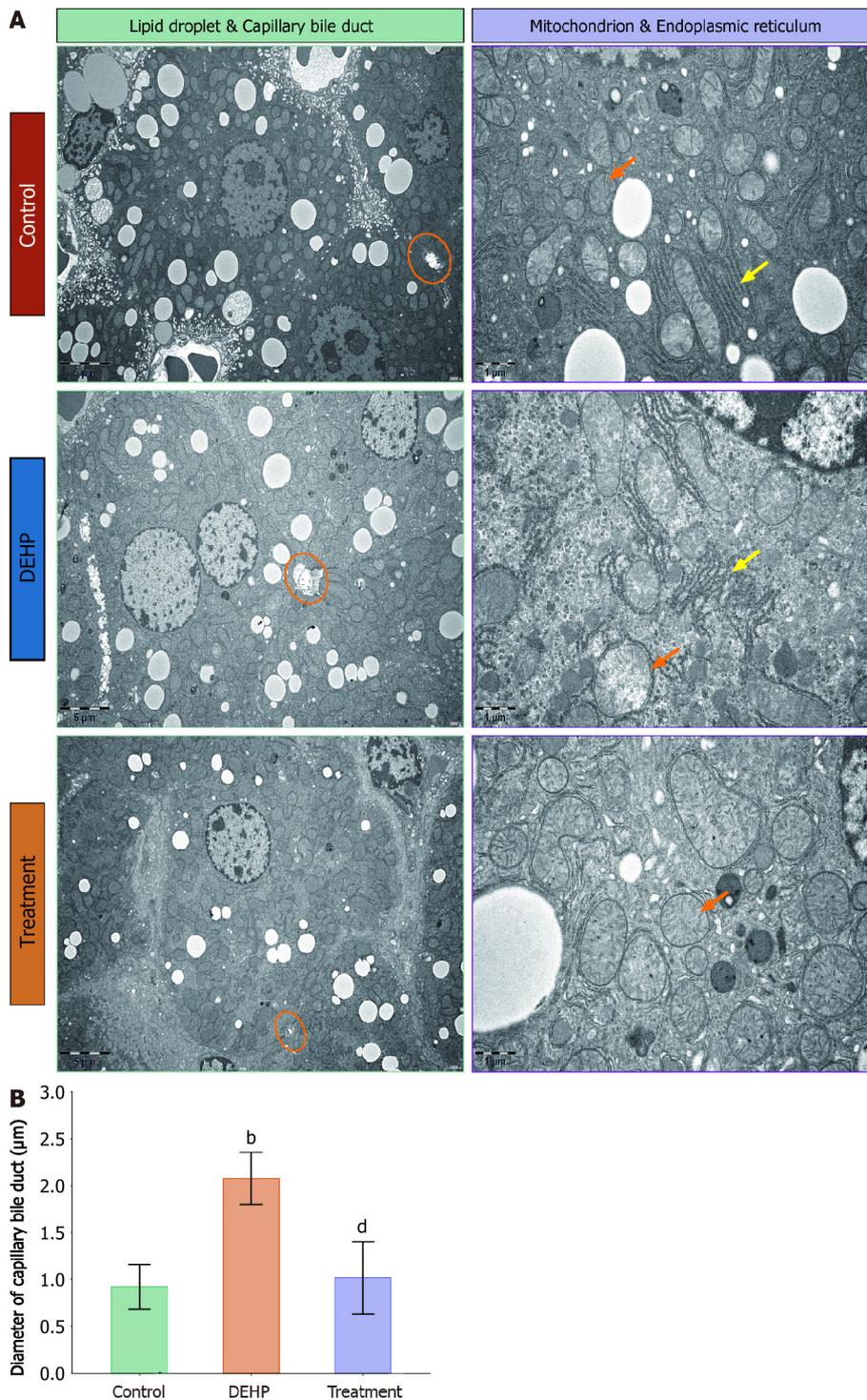
Figure 5 Comparative quantitative analysis of transmission electron microscopy results between the control, model, and treatment groups. A: Comparison of transmission electron microscopy results between the control, model, and treatment groups. In the model and control groups, increased numbers of fat droplets with enhanced size were visible. Expanded capillary bile ducts (indicated with orange circles), mildly swollen mitochondria (indicated with orange arrows), and disordered rough endoplasmic reticulum (indicated with yellow arrows) were observed in the model group. In the treatment group, the number of fat droplets decreased, capillary bile ducts appeared mostly healthy (indicated with orange circles), and mitochondrial swelling was reduced (indicated with orange arrows); B: Quantitative analysis of small bile duct diameter in mice from the control, model, and treatment groups. $^bP < 0.01$ (compared to the Control group); $^dP < 0.01$ (compared to Di (2-ethylhexyl) phthalate group). DEHP: Di (2-ethylhexyl) phthalate.

Mitochondrial organization, proteasome protein catabolic process, and oxidative phosphorylation (Figure 8A); CC term: Ribosome, ribosomal subunit, and large ribosomal subunit (Figure 8B); MF term: Structural constituent of ribosome and molecular carrier activity (Figure 8C). Additionally, the differentially expressed mRNAs in the treatment group were enriched in the following KEGG pathways: Mitochondrial autophagy, glutathione metabolism, oxidative phosphorylation, and drug metabolism (Figure 8D).
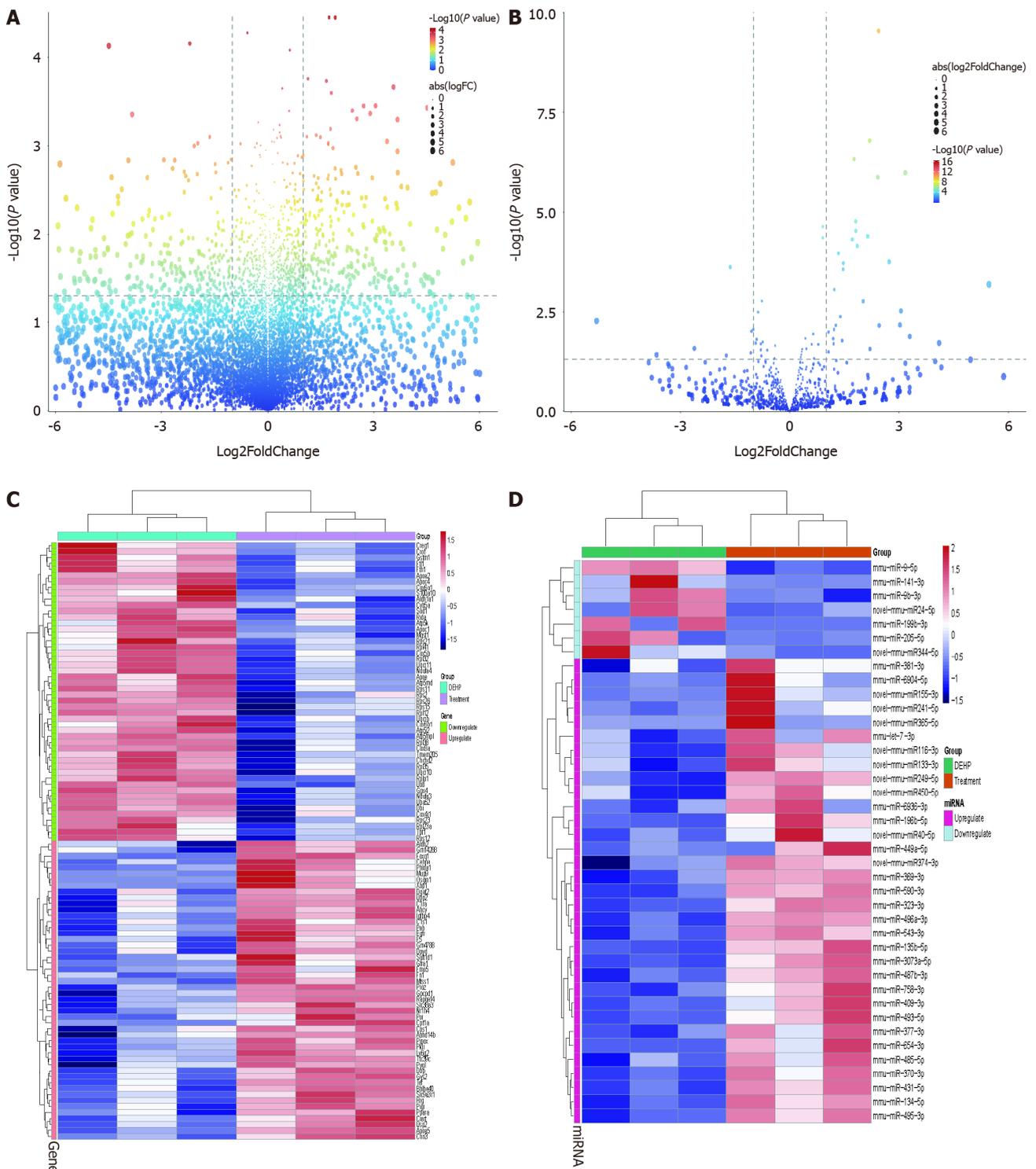
DOI: 10.3748/wjg.v29.i34.5054 **Copyright** ©The Author(s) 2023.

Figure 6 Differential expression of mRNAs and microRNAs between the treatment and model groups. A: The volcano plot of differentially expressed mRNAs between the treatment and model groups. The upper left quadrant and the upper right quadrant in the figure represent downregulated and upregulated mRNAs, respectively; B: The volcano plot of differentially expressed microRNAs (miRNAs) between the treatment and model groups. The upper left quadrant and the upper right quadrant in the figure represent downregulated and upregulated miRNAs, respectively; C: Heatmap shows the 50 mRNAs that exhibited the highest upregulation and downregulation in the treatment group relative to the model group; D: Heatmap shows the miRNAs that exhibited the highest upregulation and downregulation in the treatment group relative to the model group.

Immune infiltration analysis

The proportions and infiltration levels of immune cells in the control, model, and treatment groups are shown in Figure 9A and B. Compared with those in the control group, the infiltration levels of monocytes and immature CD8+ T cells were significantly upregulated and the infiltration levels of immature CD4+ T cells were significantly downregulated in the model group (Figure 9C). Meanwhile, compared with those in the model group, the infiltration levels of
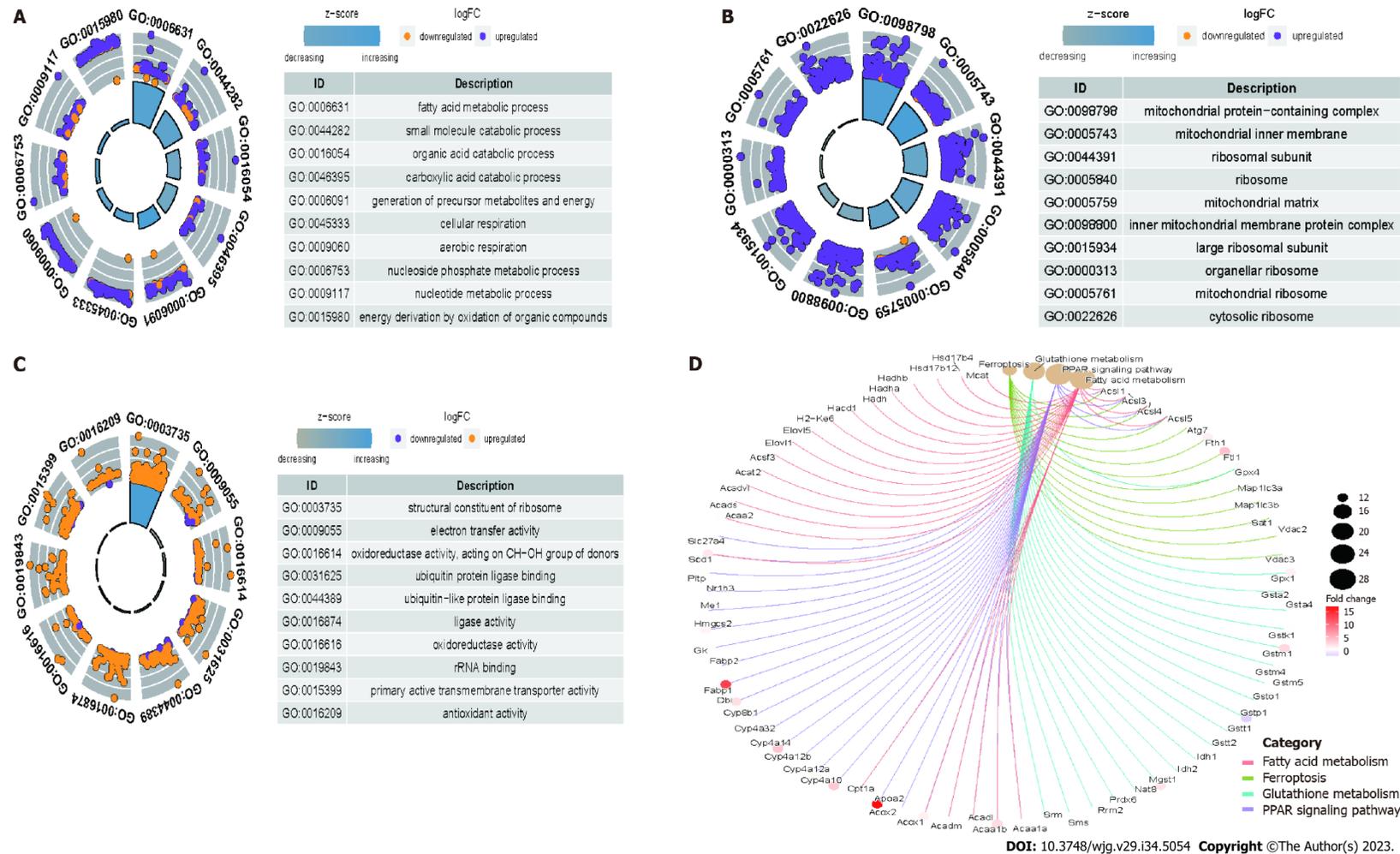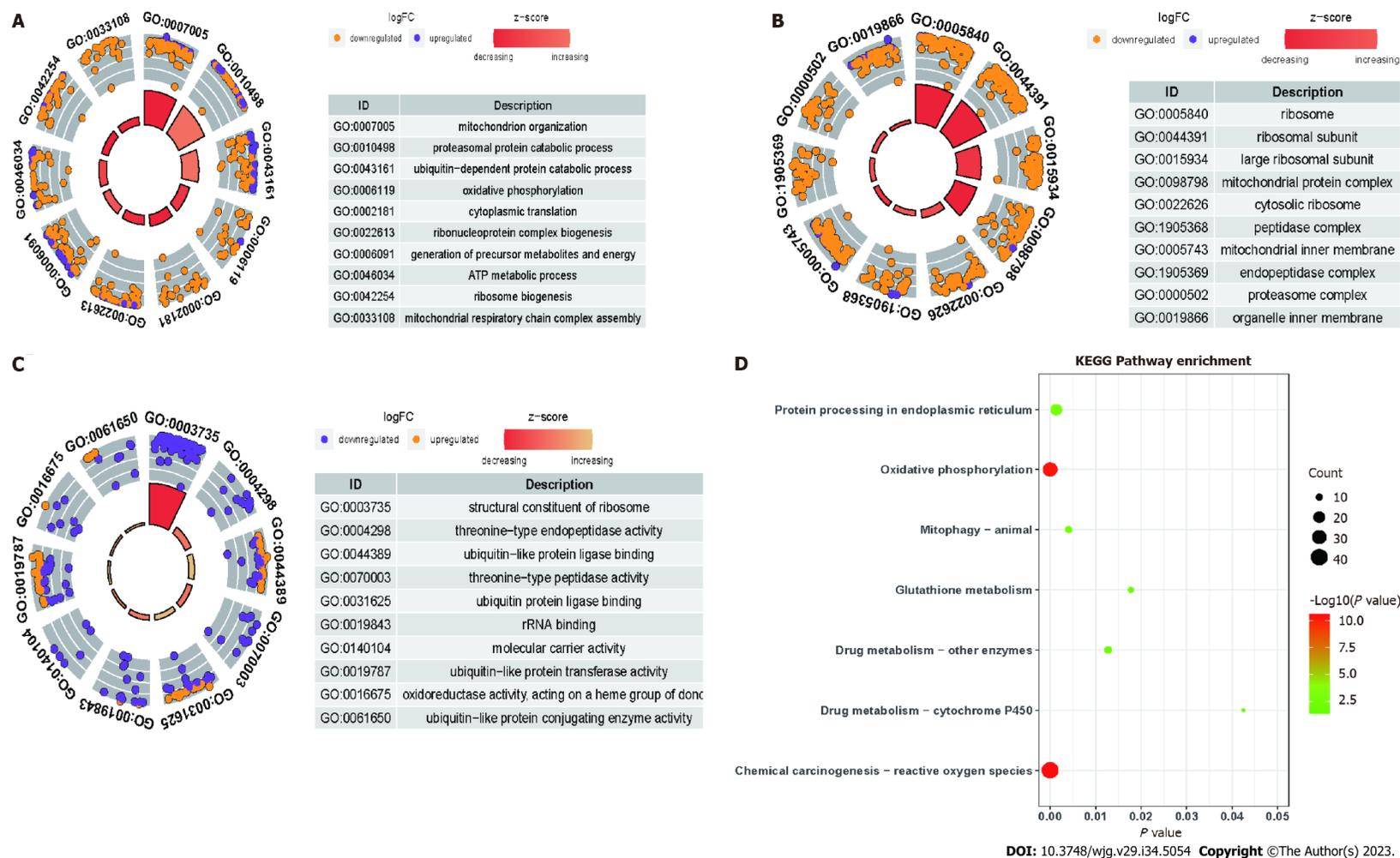
Figure 7 The differentially expressed mRNAs between the model and control groups were enriched in different Gene Ontology terms and Kyoto Encyclopedia of Genes and Genomes pathways. A: Biological processes; B: Cellular components; C: Molecular function; D: Kyoto Encyclopedia of Genes and Genomes pathways.

mast cells and active NK cells were significantly upregulated and the infiltration levels of M2 macrophages were significantly downregulated in the treatment group (Figure 9D). The correlation analysis results of various immune cells are shown in Figure 9E.

Figure 8 The differentially expressed mRNAs between the treatment and model groups were enriched in different Gene Ontology terms and Kyoto Encyclopedia of Genes and Genomes pathways. A: Biological processes; B: Cellular components; C: Molecular function; D: Kyoto Encyclopedia of Genes and Genomes pathways.

Construction of miRNA-mRNA-protein regulatory axis

Network diagrams (Figure 10A) of upregulated miRNAs and downregulated mRNAs, as well as that of downregulated miRNAs and upregulated mRNAs, in the treatment group were constructed. The data were matched with the miRNA-mRNA regulatory axis in the starBase database to obtain the mmu-miR-141-3p/Zcchc24 and mmu-miR-9-5p/Zbtb7a axes (Figure 10B). Correlation analysis (Figure 10C and D) revealed that the correlation coefficients of mmu-miR-141-3p/
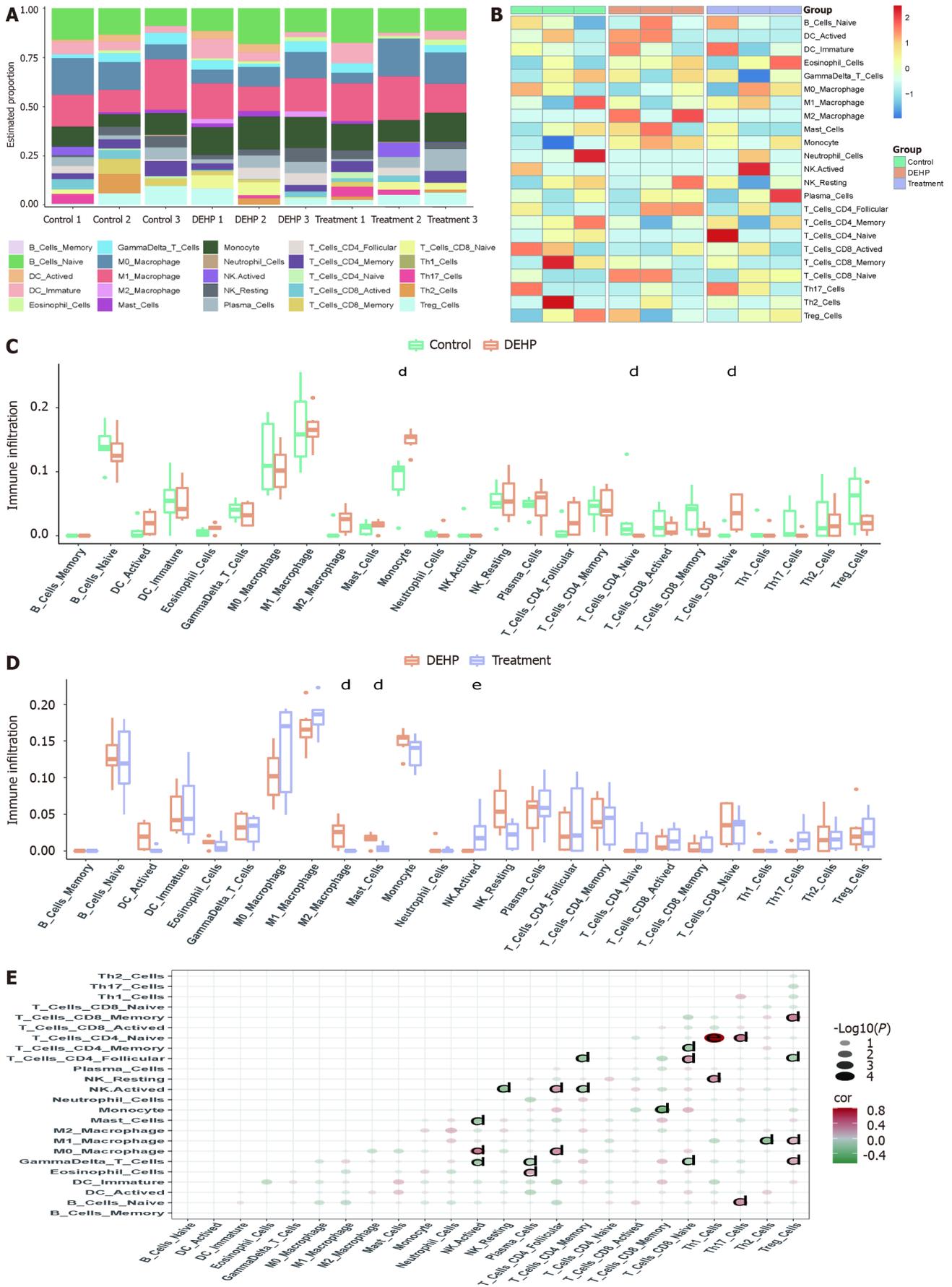
DOI: 10.3748/wjg.v29.i34.5054 **Copyright** ©The Author(s) 2023.

Figure 9 Immune infiltration analyses. A and B: Histograms (A) and heatmaps (B) of the proportions of immune cells in the control, model, and treatment groups; C and D: Analyses of differential immune cell infiltration between the model and control groups (C), as well as between the treatment and model groups (D); E:

Correlation analyses of immune cells in different groups. [d]*P* < 0.01 (compared to Di (2-ethylhexyl) phthalate group); [e]*P* < 0.05 (compared to Oil group). DEHP: Di (2-ethylhexyl) phthalate.

Zcchc24 and mmu-miR-9-5p/Zbtb7a axes were -0.44 and -0.87, respectively. To validate these regulatory axes, the liver tissues of the control, model, and treatment groups were subjected to western blotting (Figure 10E). Compared with that in the model group, the average gray value of Zcchc24 protein was significantly downregulated in the treatment group (Figure 10F), indicating that protein expression changes were consistent with mRNA expression changes. However, Zbtb7a protein expression could not be validated using western blotting or immunohistochemical analysis due to low expression levels. These findings indicate that the mmu-miR-141-3p/*Zcchc24* (mRNA)/Zcchc24 (protein) regulatory axis plays an important role in the protective effects of GTPs on DEHP-induced liver injury in mice (Figure 10G).

DISCUSSION

This study aimed to investigate the therapeutic mechanism of GTPs in alleviating DEHP-induced liver dysfunction, blood lipid dysregulation, non-alcoholic fatty liver, and liver fibrosis. Additionally, the role of a miRNA-mRNA-protein regulatory axis in the therapeutic effects of GTPs on DEHP-induced liver damage was elucidated (Figure 11). Thus, the findings of this study provide valuable insights into the potential therapeutic application of GTPs in DEHP-induced liver damage.
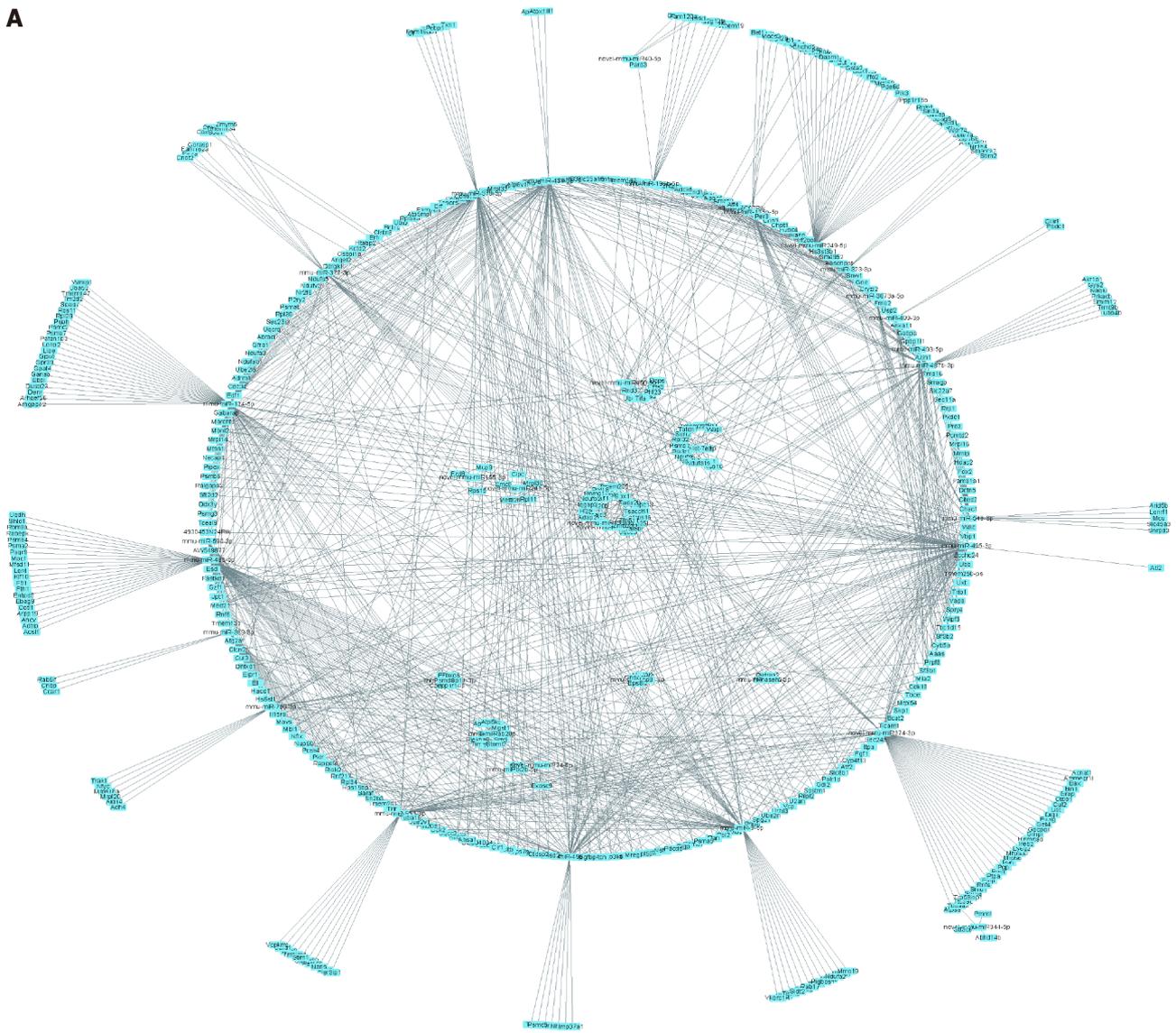
Histopathological analysis revealed that GTPs are effective in mitigating DEHP-induced non-alcoholic fatty liver disease and liver fibrosis in mice. This finding is consistent with that of previous studies, which reported the beneficial effects of GTP on liver health. For example, a meta-analysis[29] of 20 randomized controlled trials with 1536 participants revealed that green tea decreases the levels of total cholesterol and LDL. Zhao *et al*[30] reported that DEHP exposure significantly promotes inflammation, necrosis, and fibrosis in the liver and upregulates the expression of proteins associated with the development of liver inflammation and fibrosis. Kim *et al*[31] suggested that GTPs downregulate the expression of collagen content and type 1 collagen, and consequently alleviate liver fibrosis. Additionally, animal studies [32] have indicated that supplementation of green tea effectively prevented excessive accumulation of visceral and liver lipids, elevated blood glucose levels, and alleviated aberrant blood lipid levels, liver dysfunction, and hepatic steatosis in male C57BL/6 mice fed on a high-fat diet for six weeks as evidenced by the analysis of serum biochemical parameters, histological changes, lipid accumulation, inflammatory cytokines, and related indices. These findings further indicated the therapeutic potential of GTPs in liver-related conditions.

In this study, GTPs were found to ameliorate the DEHP-induced pathological damage to the liver microstructures, including the mitochondria, endoplasmic reticulum, and capillary bile ducts. These findings are consistent with those of previous studies, which reported the adverse effects of DEHP on liver microstructures. For instance, an animal study[33] indicated that DEHP induced mitochondrial and endoplasmic reticulum ultrastructural damages, characterized by increased fission and decreased fusion. Furthermore, Sun *et al*[34] suggested that DEHP promoted mitochondrial-associated endoplasmic reticulum membrane disruption, potentially through endoplasmic reticulum unfolded protein response, to induce endoplasmic reticulum stress. Consistent with the results of this study, in vitro and *in vivo* experimental studies[35] have demonstrated that GTPs effectively alleviate acetaminophen-induced liver damage and mitochondrial dysfunction. These studies have shown that GTPs possess antioxidant capacity and can prevent liver mitochondrial damage. Specifically, GTPs have been found to enhance the membrane potential and activity of liver mitochondrial respiratory chain complexes, thereby protecting against mitochondrial dysfunction. However, further research is needed to fully elucidate the underlying mechanisms and to explore the clinical applications of GTPs in protecting liver microstructures from DEHP-induced damage.
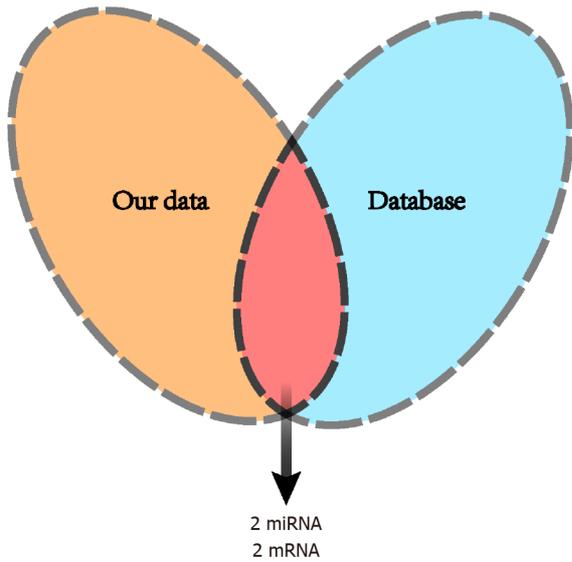
In this study, we aimed to analyze the signaling pathways involved in DEHP-induced liver damage and the hepatoprotective effects of GTPs using high-throughput sequencing. Ferroptosis, a recently discovered non-apoptotic cell death process, is induced by intracellular iron-dependent lipid peroxidation damage. Consistent with the findings of this study, Yin *et al*[36] investigated the acute toxicity of DEHP exposure in marine medaka. They conducted transcriptome analysis on the liver of DEHP-exposed medaka and reported that females were more sensitive to the immune response than males under acute DEHP exposure conditions. Furthermore, they found that DEHP exposure promoted iron depletion, leading to iron overload, increased levels of MDA and lipid peroxidation, and decreased levels of glutathione. These findings suggest that DEHP can rapidly alter certain molecular regulatory patterns and induce cell death through ferroptosis. In addition, we discussed the PPAR signaling pathway, which is a classic pathway associated with hyperlipidemia, regulates lipid metabolism and blood lipid levels by mediating various biological functions, such as the synthesis and decomposition of cholesterol and the oxidation of fatty acids[37]. Previous studies[38,39] have revealed that DEHP exposure dysregulates blood lipid levels and hepatic lipid metabolism in mice through the PPAR signaling pathway.

In this study, we utilized the CIBERSORT algorithm to identify specific alterations in immune cells. Consistent with the findings of this study, Yang *et al*[40] investigated the effect of DEHP on the immune system of male C57Bl/6 mice and reported significant atrophy of the thymus and spleen with the proportions of immature CD4+ and CD8+ populations exhibiting the highest downregulation. Additionally, they found a downregulation in the number of T and B cells in the spleen. A previous study[41] reported that green tea extract promotes macrophage phagocytic activity at a dosage of 5 mg/kg bodyweight and enhances NK cell activity and T cell proliferation at a dosage of 40 mg/kg bodyweight, supporting the potential immunomodulatory effects of GTPs demonstrated in this study.
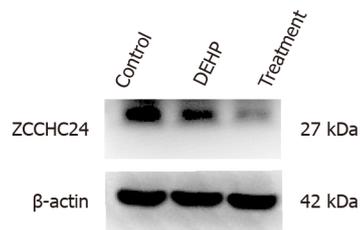
A

B

Our data

Database

2 miRNA
2 mRNA

E

	Control	DEHP	Treatment	
ZCCHC24				27 kDa
β-actin				42 kDa

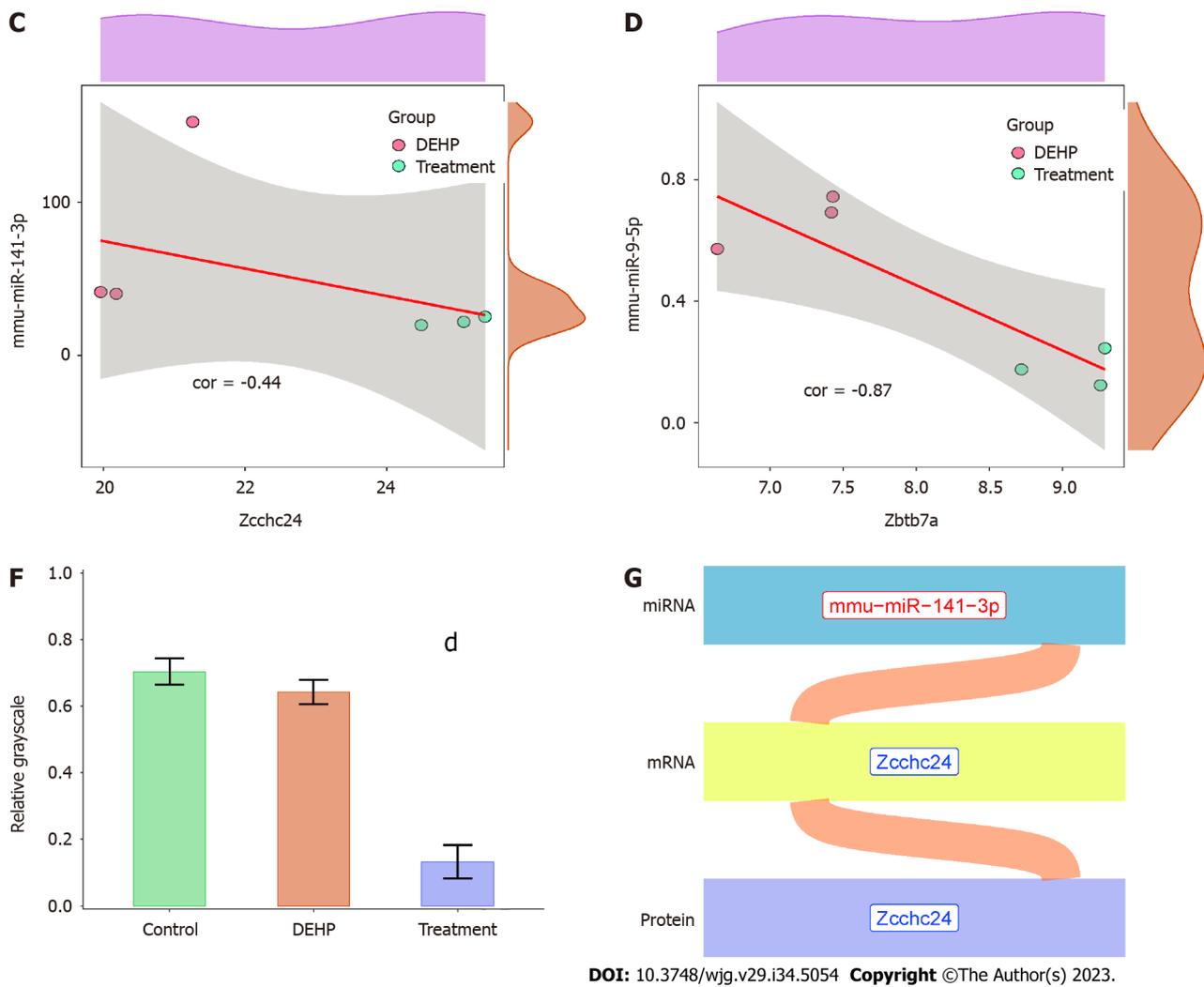**DOI:** 10.3748/wjg.v29.i34.5054 **Copyright** ©The Author(s) 2023.

Figure 10 Construction of the microRNA-mRNA-protein regulatory axis. A: The network diagram was constructed using differentially expressed mRNAs and microRNAs (miRNAs); B: Wayne diagram indicating the intersection of the miRNA-mRNA regulatory axis and mouse interaction network from the starBase database; C: Correlation analyses of mmu-miR-141-3p and Zcchc24; D: Correlation analyses of mmu-miR-9-5p and Zbtb7a; E: Western blotting validation of Zcchc24 protein expression in the control, model, and treatment groups; F: Semiquantitative analysis of Zcchc24 protein levels in the control, model, and treatment groups; G: The Sankey plot of the miRNA-mRNA-protein regulatory axes mediating the suppressive effects of green tea polyphenols (GTPs) on di-(2-ethylhexyl) phthalate (DEHP)-induced liver damage in mice. Red and blue fonts indicate upregulated and downregulated expression, respectively. $^{d}P < 0.01$ (compared to DEHP group). DEHP: Di (2-ethylhexyl) phthalate; GTPs: Green tea polyphenols.

This study identified the mmu-miR-141-3p/*Zcchc24* (mRNA)/Zcchc24 (protein) regulatory axis, which exerted its function through Zcchc24. *Zcchc24* is reported to be involved in cell differentiation in mice. Previous studies[42] have suggested that *Zcchc24* can serve as a key gene in liver cancer prediction models, which are used to predict patient survival time. Additionally, *Zcchc24* is one of the major selective splicing factors that plays a critical role in cell fate transition, development, and disease progression.

This study has several limitations. In this study, three samples per group were analyzed using high-throughput sequencing, which may have yielded biased results. Additionally, the levels of immune cells in each group were determined using the CIBERSORT algorithm. However, immune cell infiltration was not verified using alternate methods, such as single-cell sequencing. Furthermore, the importance of *Zcchc24* was not verified using knockdown or overexpression experiments.

CONCLUSION

In conclusion, this study demonstrated that GTPs can alleviate the DEHP-induced changes in liver function and lipid profiles, improve fatty liver disease and partial liver fibrosis, and regulate immune cell infiltration. Additionally, an important miRNA-mRNA-protein molecular regulation axis that plays a crucial role in the therapeutic effects of GTPs on DEHP-induced liver damage was validated.
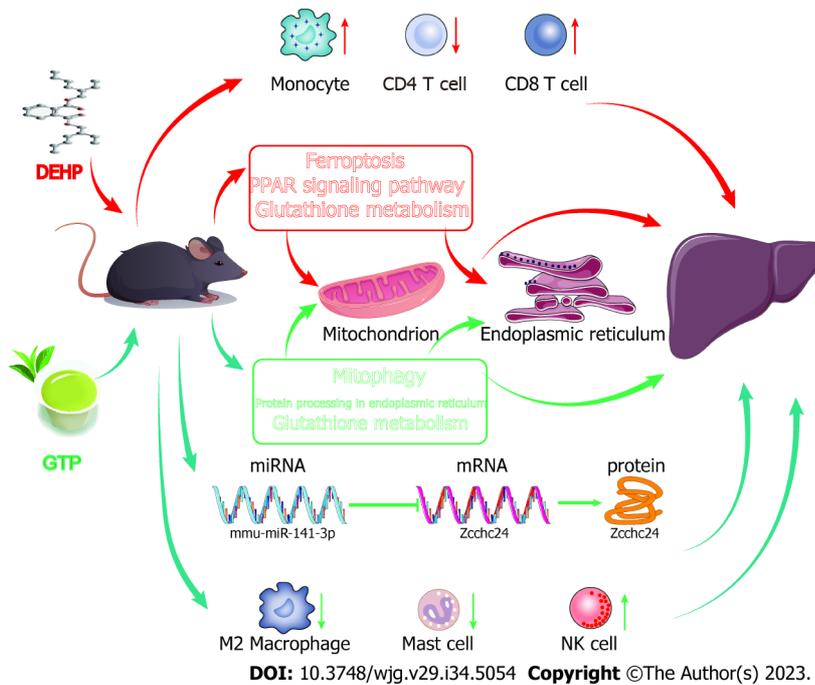
Figure 11 Mechanisms underlying di-(2-ethylhexyl) phthalate exposure-induced liver injury and the therapeutic effects of green tea polyphenols on Di (2-ethylhexyl) phthalate-indued liver injury. DEHP: Di (2-ethylhexyl) phthalate; GTPs: Green tea polyphenols.

ARTICLE HIGHLIGHTS

Research background

Di (2-ethylhexyl) phthalate (DEHP) is a widely used plasticizer that has been shown to cause liver injury. Previous studies have reported the therapeutic effects of green tea on organ damage caused by heavy metal exposure. However, there is limited research on the therapeutic effects of green tea polyphenols (GTPs) specifically on DEHP-induced liver damage.

Research motivation

Despite the known therapeutic effects of green tea on heavy metal exposure-induced organ damage, there is a lack of studies investigating the specific therapeutic effects of GTPs on DEHP-induced liver damage.

Research objectives

The research objectives of this study were to evaluate the molecular mechanism underlying the therapeutic effects of GTPs on DEHP-induced liver damage.

Research methods

In this study, C57BL/6J mice were divided into different groups and treated with DEHP and GTPs. After 8 wk, various assessments were conducted, including examination of liver function, blood lipid profile, and liver histopathology. High-throughput sequencing was used to analyze differentially expressed miRNAs and mRNAs in the liver tissues. Functional enrichment analysis and immune infiltration prediction were performed, and the miRNA-mRNA regulatory axis was elucidated using the starBase database. Protein expression was evaluated using immunohistochemistry.

Research results

The results of this study showed that GTPs had beneficial effects on DEHP-induced liver damage in mice. GTPs alleviated liver dysfunction, blood lipid dysregulation, fatty liver disease, liver fibrosis, and mitochondrial and endoplasmic reticulum lesions. The infiltration of immune cells, such as macrophages, mast cells, and natural killer cells, varied between the model and treatment groups. Furthermore, the study identified specific miRNAs, mRNAs, and proteins that constituted a regulatory axis involved in mediating the therapeutic effects of GTPs on DEHP-induced liver damage.

Research conclusions

The findings of this study indicate that GTPs have a therapeutic effect on DEHP-induced liver damage. GTPs were shown to alleviate liver dysfunction, blood lipid dysregulation, fatty liver disease, and partial liver fibrosis. Additionally, GTPs were found to regulate immune cell infiltration. The study also identified a significant miRNA-mRNA-protein regulatory axis involved in mediating the therapeutic effects of GTPs on DEHP-induced liver damage.

Research perspectives

Further studies are needed to investigate the long-term effects of GTPs on DEHP-induced liver damage and to explore the potential mechanisms underlying the regulation of immune cell infiltration. Additionally, future research should focus on optimizing the dosage and administration of GTPs to maximize their therapeutic effects and minimize potential side effects. Furthermore, clinical trials are warranted to evaluate the efficacy and safety of GTPs as a potential therapeutic intervention for DEHP-induced liver damage in humans.

ACKNOWLEDGEMENTS

FOOTNOTES

Institutional review board statement: The study does not include Human subject research.

Institutional animal care and use committee statement: All animal experiments conformed to the internationally accepted principles for the care and use of laboratory animals (licence No. IACUC-20210630-15; protocol no. 2021621-01, The Laboratory Animal Welfare and Ethic Commettee, Jinan University, Guangzhou, China).

Conflict-of-interest statement: The authors declare no competing financial interest.

Data sharing statement: The data that support the findings of this study are openly available in the NCBI GEO database at https://www.ncbi.nlm.nih.gov/geo/ with the accession number: GSE232128.

ARRIVE guidelines statement: The authors have read the ARRIVE guidelines, and the manuscript was prepared and revised according to the ARRIVE guidelines.

Country/Territory of origin: China

ORCID number: Qin Peng 0000-0001-6243-3416; Sheng-Yun Sun 0000-0002-0374-8482.

S-Editor: Fan JR
L-Editor: A
P-Editor: Yuan YY

REFERENCES

1   **Liu Y**, Guo Z, Zhu R, Gou D, Jia PP, Pei DS. An insight into sex-specific neurotoxicity and molecular mechanisms of DEHP: A critical review. *Environ Pollut* 2023; **316**: 120673 [PMID: 36400143 DOI: 10.1016/j.envpol.2022.120673]

2   **Erythropel HC**, Maric M, Nicell JA, Leask RL, Yargeau V. Leaching of the plasticizer di(2-ethylhexyl)phthalate (DEHP) from plastic containers and the question of human exposure. *Appl Microbiol Biotechnol* 2014; **98**: 9967-9981 [PMID: 25376446 DOI: 10.1007/s00253-014-6183-8]

3   **Silva MJ**, Wong LY, Samandar E, Preau JL, Calafat AM, Ye X. Exposure to di-2-ethylhexyl terephthalate in a convenience sample of U.S. adults from 2000 to 2016. *Arch Toxicol* 2017; **91**: 3287-3291 [PMID: 28314884 DOI: 10.1007/s00204-017-1956-3]

4   **Kavlock R**, Boekelheide K, Chapin R, Cunningham M, Faustman E, Foster P, Golub M, Henderson R, Hinberg I, Little R, Seed J, Shea K, Tabacova S, Tyl R, Williams P, Zacharewski T. NTP Center for the Evaluation of Risks to Human Reproduction: phthalates expert panel report on the reproductive and developmental toxicity of di-n-octyl phthalate. *Reprod Toxicol* 2002; **16**: 721-734 [PMID: 12406498 DOI: 10.1016/s0890-6238(02)00031-x]

5   **Chen L**, Zhao Y, Li L, Chen B, Zhang Y. Exposure assessment of phthalates in non-occupational populations in China. *Sci Total Environ* 2012; **427-428**: 60-69 [PMID: 22578696 DOI: 10.1016/j.scitotenv.2012.03.090]

6   **Matsumoto M**, Hirata-Koizumi M, Ema M. Potential adverse effects of phthalic acid esters on human health: a review of recent studies on reproduction. *Regul Toxicol Pharmacol* 2008; **50**: 37-49 [PMID: 17983696 DOI: 10.1016/j.yrtph.2007.09.004]

7   **Jadeja RN**, Urrunaga NH, Dash S, Khurana S, Saxena NK. Withaferin-A Reduces Acetaminophen-Induced Liver Injury in Mice. *Biochem Pharmacol* 2015; **97**: 122-132 [PMID: 26212553 DOI: 10.1016/j.bcp.2015.07.024]

8   **Chen H**, Zhang W, Rui BB, Yang SM, Xu WP, Wei W. Di(2-ethylhexyl) phthalate exacerbates non-alcoholic fatty liver in rats and its potential mechanisms. *Environ Toxicol Pharmacol* 2016; **42**: 38-44 [PMID: 26773359 DOI: 10.1016/j.etap.2015.12.016]

9   **Yang G**, Zhang W, Qin Q, Wang J, Zheng H, Xiong W, Yuan J. Mono(2-ethylhexyl) phthalate induces apoptosis in p53-silenced L02 cells *via* activation of both mitochondrial and death receptor pathways. *Environ Toxicol* 2015; **30**: 1178-1191 [PMID: 24706461 DOI: 10.1002/tox.21990]

10   **Isenberg JS**, Kamendulis LM, Smith JH, Ackley DC, Pugh G Jr, Lington AW, Klaunig JE. Effects of Di-2-ethylhexyl phthalate (DEHP) on gap-junctional intercellular communication (GJIC), DNA synthesis, and peroxisomal beta oxidation (PBOX) in rat, mouse, and hamster liver. *Toxicol Sci* 2000; **56**: 73-85 [PMID: 10869455 DOI: 10.1093/toxsci/56.1.73]

11   **Ray PD**, Huang BW, Tsuji Y. Reactive oxygen species (ROS) homeostasis and redox regulation in cellular signaling. *Cell Signal* 2012; **24**: 981-990 [PMID: 22286106 DOI: 10.1016/j.cellsig.2012.01.008]

12   **Santhosh A**, Nair KG, Arun P, Deepadevi KV, Manojkumar V, Lakshmi LR, Kurup PA. Effect of DEHP [di-(2-ethyl hexyl) phthalate] on lipid peroxidation in liver in rats and in primary cultures of rat hepatocytes. *Indian J Med Res* 1998; **108**: 17-23 [PMID: 9745214]

13   **Ghosh J**, Das J, Manna P, Sil PC. Hepatotoxicity of di-(2-ethylhexyl)phthalate is attributed to calcium aggravation, ROS-mediated mitochondrial depolarization, and ERK/NF-κB pathway activation. *Free Radic Biol Med* 2010; **49**: 1779-1791 [PMID: 20854900 DOI: 10.1016/j.freeradbiomed.2010.09.011]

14   **Afzal M**, Safer AM, Menon M. Green tea polyphenols and their potential role in health and disease. *Inflammopharmacology* 2015; **23**: 151-161 [PMID: 26164000 DOI: 10.1007/s10787-015-0236-1]

15   **Mukhtar H**, Ahmad N. Tea polyphenols: prevention of cancer and optimizing health. *Am J Clin Nutr* 2000; **71**: 1698S-702S; discussion 1703S [PMID: 10837321 DOI: 10.1093/ajcn/71.6.1698S]

16   **Nagao T**, Hase T, Tokimitsu I. A green tea extract high in catechins reduces body fat and cardiovascular risks in humans. *Obesity (Silver Spring)* 2007; **15**: 1473-1483 [PMID: 17557985 DOI: 10.1038/oby.2007.176]

17   **Huang J**, Wang Y, Xie Z, Zhou Y, Zhang Y, Wan X. The anti-obesity effects of green tea in human intervention and basic molecular studies. *Eur J Clin Nutr* 2014; **68**: 1075-1087 [PMID: 25074392 DOI: 10.1038/ejcn.2014.143]

18   **Zwolak I**. Epigallocatechin Gallate for Management of Heavy Metal-Induced Oxidative Stress: Mechanisms of Action, Efficacy, and Concerns. *Int J Mol Sci* 2021; **22** [PMID: 33919748 DOI: 10.3390/ijms22084027]

19   **Zhao Z**, Lin CY, Cheng K. siRNA- and miRNA-based therapeutics for liver fibrosis. *Transl Res* 2019; **214**: 17-29 [PMID: 31476281 DOI: 10.1016/j.trsl.2019.07.007]

20   **El-Maraghy SA**, Adel O, Zayed N, Yosry A, El-Nahaas SM, Gibriel AA. Circulatory miRNA-484, 524, 615 and 628 expression profiling in HCV mediated HCC among Egyptian patients; implications for diagnosis and staging of hepatic cirrhosis and fibrosis. *J Adv Res* 2020; **22**: 57-66 [PMID: 31956442 DOI: 10.1016/j.jare.2019.12.002]

21   **Lin Q**, Zhou CR, Bai MJ, Zhu D, Chen JW, Wang HF, Li MA, Wu C, Li ZR, Huang MS. Exosome-mediated miRNA delivery promotes liver cancer EMT and metastasis. *Am J Transl Res* 2020; **12**: 1080-1095 [PMID: 32269736]

22   **Sanjay S**, Girish C. Role of miRNA and its potential as a novel diagnostic biomarker in drug-induced liver injury. *Eur J Clin Pharmacol* 2017; **73**: 399-407 [PMID: 28028586 DOI: 10.1007/s00228-016-2183-1]

23   **Hou P**, Dai W, Jin Y, Zhao F, Liu J, Liu H. Maternal exposure to di-2-ethylhexyl phthalate (DEHP) depresses lactation capacity in mice. *Sci Total Environ* 2022; **837**: 155813 [PMID: 35550907 DOI: 10.1016/j.scitotenv.2022.155813]

24   **XueXia L**, YaNan L, Zi T, YuSheng Z, ZeLin W, Peng Z, MeiNa X, FuJun L. Di-2-ethylhexyl phthalate (DEHP) exposure induces sperm quality and functional defects in mice. *Chemosphere* 2023; **312**: 137216 [PMID: 36372335 DOI: 10.1016/j.chemosphere.2022.137216]

25   **Zhou X**, Zhang Z, Shi H, Liu Q, Chang Y, Feng W, Zhu S, Sun S. Effects of Lycium barbarum glycopeptide on renal and testicular injury induced by di(2-ethylhexyl) phthalate. *Cell Stress Chaperones* 2022; **27**: 257-271 [PMID: 35362893 DOI: 10.1007/s12192-022-01266-0]

26   **Abdelrazek HM**, Helmy SA, Elsayed DH, Ebaid HM, Mohamed RM. Ameliorating effects of green tea extract on cadmium induced reproductive injury in male Wistar rats with respect to androgen receptors and caspase- 3. *Reprod Biol* 2016; **16**: 300-308 [PMID: 27840064 DOI: 10.1016/j.repbio.2016.11.001]

27   **Newman AM**, Liu CL, Green MR, Gentles AJ, Feng W, Xu Y, Hoang CD, Diehn M, Alizadeh AA. Robust enumeration of cell subsets from tissue expression profiles. *Nat Methods* 2015; **12**: 453-457 [PMID: 25822800 DOI: 10.1038/nmeth.3337]

28   **Chen Z**, Huang A, Sun J, Jiang T, Qin FX, Wu A. Inference of immune cell composition on the expression profiles of mouse tissue. *Sci Rep* 2017; **7**: 40508 [PMID: 28084418 DOI: 10.1038/srep40508]

29   **Onakpoya I**, Spencer E, Heneghan C, Thompson M. The effect of green tea on blood pressure and lipid profile: a systematic review and meta-analysis of randomized clinical trials. *Nutr Metab Cardiovasc Dis* 2014; **24**: 823-836 [PMID: 24675010 DOI: 10.1016/j.numecd.2014.01.016]

30   **Zhao ZB**, Ji K, Shen XY, Zhang WW, Wang R, Xu WP, Wei W. Di(2-ethylhexyl) phthalate promotes hepatic fibrosis by regulation of oxidative stress and inflammation responses in rats. *Environ Toxicol Pharmacol* 2019; **68**: 109-119 [PMID: 30884453 DOI: 10.1016/j.etap.2019.03.008]

31   **Kim HK**, Yang TH, Cho HY. Antifibrotic effects of green tea on in vitro and in vivo models of liver fibrosis. *World J Gastroenterol* 2009; **15**: 5200-5205 [PMID: 19891020 DOI: 10.3748/wjg.15.5200]

32   **Zhou J**, Yu Y, Ding L, Xu P, Wang Y. Matcha Green Tea Alleviates Non-Alcoholic Fatty Liver Disease in High-Fat Diet-Induced Obese Mice by Regulating Lipid Metabolism and Inflammatory Responses. *Nutrients* 2021; **13** [PMID: 34204055 DOI: 10.3390/nu13061950]

33   **Zhao Y**, Cui JG, Zhang H, Li XN, Li MZ, Talukder M, Li JL. Role of mitochondria-endoplasmic reticulum coupling in lycopene preventing DEHP-induced hepatotoxicity. *Food Funct* 2021; **12**: 10741-10749 [PMID: 34608470 DOI: 10.1039/d1fo00478f]

34   **Sun X**, Lin Y, Huang Q, Shi J, Qiu L, Kang M, Chen Y, Fang C, Ye T, Dong S. Di(2-ethylhexyl) phthalate-induced apoptosis in rat INS-1 cells is dependent on activation of endoplasmic reticulum stress and suppression of antioxidant protection. *J Cell Mol Med* 2015; **19**: 581-594 [PMID: 25418486 DOI: 10.1111/jcmm.12409]

35   **Lin Y**, Huang J, Gao T, Wu Y, Huang D, Yan F, Weng Z. Preliminary Study on Hepatoprotective Effect and Mechanism of (-)-

Epigallocatechin-3-gallate against Acetaminophen-induced Liver Injury in Rats. *Iran J Pharm Res* 2021; **20**: 46-56 [PMID: 34903968 DOI: 10.22037/ijpr.2020.112727.13918]

36   **Yin X**, Zeb R, Wei H, Cai L. Acute exposure of di(2-ethylhexyl) phthalate (DEHP) induces immune signal regulation and ferroptosis in oryzias melastigma. *Chemosphere* 2021; **265**: 129053 [PMID: 33272674 DOI: 10.1016/j.chemosphere.2020.129053]

37   **Giordano Attianese GM**, Desvergne B. Integrative and systemic approaches for evaluating PPARβ/δ (PPARD) function. *Nucl Recept Signal* 2015; **13**: e001 [PMID: 25945080 DOI: 10.1621/nrs.13001]

38   **Zhang Y**, Ge S, Yang Z, Li Z, Gong X, Zhang Q, Dong W, Dong C. Disturbance of di-(2-ethylhexyl) phthalate in hepatic lipid metabolism in rats fed with high fat diet. *Food Chem Toxicol* 2020; **146**: 111848 [PMID: 33166671 DOI: 10.1016/j.fct.2020.111848]

39   **Xu M**, Li Y, Wang X, Zhang Q, Wang L, Zhang X, Cui W, Han X, Ma N, Li H, Fang H, Tang S, Li J, Liu Z, Yang H, Jia X. Role of Hepatocyte- and Macrophage-Specific PPARγ in Hepatotoxicity Induced by Diethylhexyl Phthalate in Mice. *Environ Health Perspect* 2022; **130**: 17005 [PMID: 35019730 DOI: 10.1289/EHP9373]

40   **Yang Q**, Xie Y, Depierre JW. Effects of peroxisome proliferators on the thymus and spleen of mice. *Clin Exp Immunol* 2000; **122**: 219-226 [PMID: 11091278 DOI: 10.1046/j.1365-2249.2000.01367.x]

41   **Huang AC**, Cheng HY, Lin TS, Chen WH, Lin JH, Lin JJ, Lu CC, Chiang JH, Hsu SC, Wu PP, Huang YP, Chung JG. Epigallocatechin gallate (EGCG), influences a murine WEHI-3 leukemia model in vivo through enhancing phagocytosis of macrophages and populations of T- and B-cells. *In Vivo* 2013; **27**: 627-634 [PMID: 23988898]

42   **Apizi A**, Wang L, Wusiman L, Song E, Han Y, Jia T, Zhang W. Establishment and verification of a prognostic model of liver cancer by RNA-binding proteins based on the TCGA database. *Transl Cancer Res* 2022; **11**: 1925-1937 [PMID: 36249884 DOI: 10.21037/tcr-21-2820]